

DYNAMIC RESPONSE OF A CRACKED VISCOELASTIC  
ANISOTROPIC PLANE USING BOUNDARY ELEMENTS AND  
FRACTIONAL DERIVATIVES

TSVIATKO V. RANGELOV<sup>1\*</sup>, PETIA S. DINEVA<sup>2</sup>,  
GEORGE D. MANOLIS<sup>3</sup>

<sup>1</sup>*Institute of Mathematics and Informatics, Bulgarian Academy of Sciences,  
Sofia 1113, Bulgaria*

<sup>2</sup>*Institute of Mechanics, Bulgarian Academy of Sciences, Sofia 1113, Bulgaria*

<sup>3</sup>*Department of Civil Engineering, Aristotle University, Thessaloniki,  
GR-54124, Greece*

[Received 31 October 2017. Accepted 11 January 2018]

**ABSTRACT:** The aim of this study is to develop an efficient numerical technique using the non-hypersingular, traction boundary integral equation method (BIEM) for solving wave propagation problems in an anisotropic, viscoelastic plane with cracks. The methodology can be extended from the macro-scale with certain modifications to the nano-scale. Furthermore, the proposed approach can be applied to any type of anisotropic material insofar as the BIEM formulation is based on the fundamental solution of the governing wave equation derived for the case of general anisotropy. The following examples are solved: (i) a straight crack in a viscoelastic orthotropic plane, and (ii) a blunt nano-crack inside a material of the same type. The mathematical modelling effort starts from linear fracture mechanics, and adds the fractional derivative concept for viscoelastic wave propagation, plus the surface elasticity model of M. E. Gurtin and A. I. Murdoch, which leads to nonclassical boundary conditions at the nano-scale. Conditions of plane strain are assumed to hold. Following verification of the numerical scheme through comparison studies, further numerical simulations serve to investigate the dependence of the stress intensity factor (SIF) and of the stress concentration factor (SCF) that develop in a cracked inhomogeneous plane on (i) the degree of anisotropy, (ii) the presence of viscoelasticity, (iii) the size effect with the associated surface elasticity phenomena, and (iv) finally the type of the dynamic disturbance propagating through the bulk material.

**KEY WORDS:** In-plane waves, viscoelasticity, fractional derivatives, anisotropy, cracks, nano-scale, surface elasticity, boundary elements, SIF, SCF.

---

\*Corresponding author e-mail: rangelov@math.bas.bg

## 1 INTRODUCTION

In order to accurately describe wave propagation in materials, attenuation and dispersion phenomena should be taken into account. Viscoelasticity is considered as the basic material model for describing these phenomena when studying elastic waves in different types of materials, both man-made (rubbers, polymers, composites) and natural (soil, rocks, biological tissues). In this respect, fractional derivatives comprise a family of advanced viscoelastic models that have been successfully introduced to describe the dynamic behaviour of complex dissipative systems in geophysics, biology, chemistry, material science, etc.

There are two basic viscoelastic formulations, see [2], first proposed by [3] and much later on by [4] for stress-strain constitutive laws that take into account wave dispersion and attenuation. The first one uses an integral equation of the hereditary type with relaxation or creep functions as the kernel functions. The second one expresses the stress-strain constitutive relations as differential equations. Linear viscoelastic models have been presented in detail by [5] and [6]. The first dynamic viscoelastic boundary element method (BEM) formulations and corresponding solutions appeared in the frequency domain [7] and in the Laplace domain [8] by using the elastic-viscoelastic correspondence principle. The complex moduli concept underlying the correspondence principle was later extended to fractional viscoelasticity by allowing fractional powers of the frequency (or the Laplace transform parameter), see [9–12]. In general, formulations using fractional derivatives proposed so far fall into two main groups: the Riemann-Liouville and Grunwald-Letnikov derivatives [13] and the Caputo derivatives [14]. The time fractional derivative is easiest to define in the frequency domain due to the property of the Fourier transform  $F$  of the  $n$ -th order derivative:  $F\left(\frac{d^n u(t)}{dt^n}\right) = (i\omega)^n U(\omega)$ , where  $U(\omega)$  is the Fourier transform of a differentiable function  $u(t)$  in time and  $\omega$  is the frequency. The fractional derivative of arbitrary order  $\alpha$ ,  $Re\alpha > 0$  can be understood as a generalization of the conventional derivative with integer  $n$  replaced by a real number  $\alpha$ . Thus, a differential equation is defined as fractional if it involves an operator that can be considered to be between the  $(k - 1)$ -th and  $k$ -th order differential operator, for positive integer  $k$ . Such fractional-order equations appear in a surprising number of real world models. One of these is the fractional Zener model, i.e. the fractional alternative to the standard linear solid, proposed by [15] and discussed in detail in [16].

Next, the wave equation can be generalized within the theory of fractional calculus by replacing second-order derivatives (space and/or time) with the fractional. The space-time fractional Zener wave equation represents a generalization of the classical elastodynamic equation, which is obtained as a system comprising the equation of motion, the time-fractional Zener constitutive law and the space-fractional strain

measure, see [17]. More specifically, the fractional Kelvin-Voigt wave equation is one of the oldest fractional wave equations in use [18], while the fractional Zener model can be considered as its extension. We refer to [19] for a review on the fractional models in dynamic viscoelasticity and to [20] for a systematic analysis of the thermodynamical restrictions on the numerical values of the parameters used in these models. Many authors among them [17, 21, 22] discussed the efficiency of the fractal derivative models to describe creep and stress relaxation in viscoelastic materials.

Most of the results available today study the influence of viscoelasticity on the scattered elastic wave far-field, while are few studies on the sensitivity of the stress intensity factors developing near the crack-tips for fractured viscoelastic materials described by different fractional constitutive laws. The applicability of the fractional derivative models for solution of dynamic problems in the frame of the linear fracture mechanics is discussed in [23, 24]. It is well known that the presence of cracks modifies traveling elastic wave fields because of diffraction, and also causes localized stress concentration phenomena. Due to this fact, numerical modeling of wave motion in a cracked continuum requires hybrid-type methodologies that combine elastodynamics with fracture mechanics. Since analytical solutions for dynamic crack problems can be obtained for simple cases only, numerical methods have to be applied to solve meaningful boundary value problems (BVP). Among the computational methods used, the BIEM has become popular for a set of reasons discussed in detail in the literature [8, 25, 26]. A recent review of BIEM modeling of wave propagation phenomena in elastic solids with cracks at the macro-level can be found in [27].

With the rapid development of nano-mechanical systems, size-dependent phenomena in the scattered wave fields, as well as local stress concentration fields in nano-structures with defects (e.g., cavities, inclusions and cracks) have attracted considerable attention. The manifestation of surface energy of the nano-level is caused by the fact that the bonds of the surface atoms are relaxed, which lead to formation of surface residual stress. Such specific behavior is termed the surface stress effect and a rational mechanical model was introduced by [1, 28, 29]. In the aforementioned model, the interfaces between the nano-inhomogeneity and the matrix are regarded as thin material surfaces which possess their own mechanical properties and surface tension. For objects with sizes greater than 100nm, the surface-to-volume ratio is negligible and the effective material properties are governed by classical bulk elastic strain energy through a fourth-order elastic stiffness tensor. A short review of results limited to 2D problems for materials with cavities, inclusions and cracks at the nano-scale, under both static and dynamic loads follows. In terms of semi-analytical methods for this class of problems, we briefly mention here the wave function expansion and the complex variable methods used to study (i) nano-holes under static anti-plane [30], static in-plane [31–34], dynamic anti-plane [35] and dynamic in-

plane [36–40] loads and conditions; (ii) nano-inclusions under static anti-plane [30], static in-plane [41,42], dynamic anti-plane [35,39,43] and dynamic in-plane, [44,45] loads and conditions; (iii) nano-cracks under static anti-plane [30,46] and static in-plane [47,48] loads and conditions.

Moving on to fully numerical solutions, recent developments in this field can be grouped as follows: (i) nano-holes under in-plane static [49–51] and in-plane dynamic [52–54] loads and conditions; (ii) nano-inclusions under in-plane static [50, 51] and in-plane dynamic loads [52, 53]; (iii) wave scattering problems by in-plane nano-cracks [55]; iv) as far as nanomechanics is concerned, one must mention the finite element method (FEM) results for in-plane blunt nano-cracks under static loads, as discussed in [56–59].

The conclusions that can now be drawn are as follows: (i) To date, there is a lack of results for surface elasticity effects on the stress fields that develop near crack-tips. (ii) At a macroscopic scale, the crack front profile is considered to be infinitely sharp and the corresponding elastic and elasto-plastic, near-field zones are well understood in the classical fracture mechanics literature. However, in reality the crack-tips are not ideally sharp but blunt with a curvature radius in the order of microns or nanometers. Experiments and simulations by atomic models [60] have shown that the stresses obtained via the atomic models are in a good agreement with the predictions of linear fracture mechanics, except in a very small vicinity around the crack-tip, where the effect of surface elastic energy should be accounted for. (iii) Furthermore, there is paucity of results for in-plane nano-cracks in elastic isotropic/anisotropic continua under dynamic loads, except for some recent work by [55] for a blunt crack in an anisotropic plane under incident time-harmonic P- and SV- wave. (iv) Finally, no results are available for either macro- or nano- cracks in viscoelastic anisotropic continua where viscous effects are represented by the Zener type model using fractal derivatives in the constitutive law for the case of dynamic loads.

The above observations serve as motivation to examine time harmonic, in-plane wave propagation in a cracked viscoelastic and orthotropic plane, so as to evaluate stress concentration fields near cracks at both macro- and nano- scales. Briefly, the paper is organized as follows: Section 2 gives the in-plane elastodynamic problem formulation for a finite crack at both the macro- and the nano-scales in a viscoelastic medium described by the Zener model with fractional derivatives in time. The medium is an orthotropic plane under incident, time-harmonic plane waves. The problem is then reformulated in Section 3 using boundary integral equations (BIE). In addition, the fundamental solution for the governing fractional viscoelastic wave equation is also presented in Section 3. Next, a series of parametric studies, including those necessary for the verification of the methodology, is presented in Section 4. This is finally followed by some conclusions in Section 5.

## 2 PROBLEM STATEMENT

Consider a homogeneous viscoelastic and orthotropic plane  $x_3 = 0$  in a Cartesian coordinate system  $Ox_1x_2x_3$ . Either a single finite line crack  $\Gamma = \Gamma^+ \cup \Gamma^-$  with length  $|\Gamma| = 2c$ , (see Fig. 1a) or a nano-crack, in domain  $G$  with boundary  $S$ , (see Fig. 1b) and perimeter  $|S| = 2[2(c - d) + \pi d]$  are embedded in the plane, which swept by P- or SV-time-harmonic waves with frequency  $\omega$  and incident angle  $\varphi$  with respect to the  $Ox_1$  axis. The nano-crack is considered as a blunt crack with boundary  $S = S^+ \cup S^- \cup S^l \cup S^r$ , where  $S^+$  and  $S^-$  are the upper and lower flat part of the blunt crack, while the crack tips are represented as semicircles  $S^l, S^r$  of radius  $d$  with values falling in the interval  $10^{-7} \text{ m} \div 10^{-10} \text{ m}$ . In the case of plane strain, the

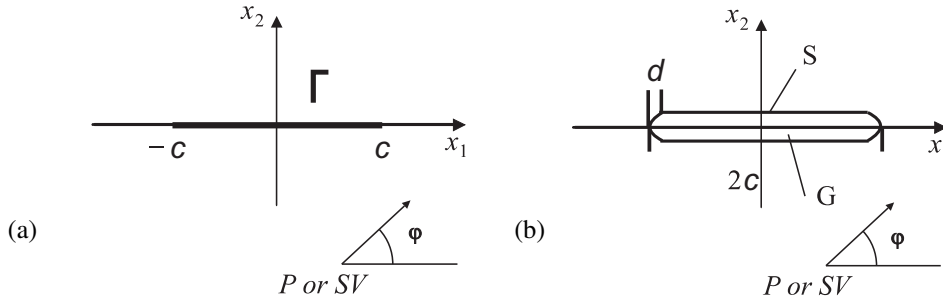


Fig. 1. Finite crack in a viscoelastic orthotropic plane under incident time-harmonic waves: a) macro-crack as an open segment; b) blunt nano-crack.

displacement components are  $u_i(x, \omega)$ ,  $i = 1, 2$ , the stress components are  $\sigma_{ij}(x, \omega)$ , the strain components are  $\varepsilon_{ij}(x, \omega)$  and the tractions are  $t_i(x, \omega) = \sigma_{ij}(x, \omega)n_j$ . Here,  $n_j$  are the components of the outward pointing unit normal vector to either the crack line  $\Gamma$  or the boundary  $S$ , while the observer point is  $x = (x_1, x_2)$ . In what follows, we define the BVP in the frequency domain in terms of the governing equations and their corresponding boundary conditions.

### 2.1 CONSTITUTIVE LAW AND STRAIN-DISPLACEMENT RELATIONS

The constitutive law employed used here is the Zener viscoelastic model with fractional time derivatives of order  $\alpha$  in the frequency domain, see [61]

$$(1) \quad (1 + a(i\omega)^\alpha)\sigma_{ij}(x, \omega) = C_{ijkl}(1 + b(i\omega)^\alpha)\varepsilon_{kl}(x, \omega).$$

In the above,  $C_{ijkl}$  is a positive definite, elastic anisotropic stiffness tensor with the following symmetry properties  $C_{ijkl} = C_{jikl} = C_{ijlk} = C_{klij}$ ,  $i, j, k, l = 1, 2$ . Also,  $a \geq 0, b \geq 0, \alpha \in [0, 1]$  are the model coefficients.

If  $\alpha = 0$  or  $a = b$ , then the Zener model (1) degenerates to Hooke's law for anisotropic materials, while if  $\alpha = 1, a \neq b$ , we have the classical Zener model,

i.e. the rheological model for the standard linear solid. The derivative order denoted by  $\alpha$  has no physical meaning, e.g., it simply acts as an interpolate between two ascending order derivatives. For instance, parameter  $\alpha$  in a single degree-of freedom representation of nonlinear base isolation systems interpolates between the zero and the first order time derivatives appearing in the equation of motion, see [62]. A best-fit (or optimal) value for  $\alpha$  can only be estimated by recourse to experimentally obtained data.

When we consider an orthotropic plane, the independent material constants are four, namely  $c_{11}, c_{12}, c_{22}, c_{66}$ , when the coordinate axis  $Ox_2$  and the principal axis of the material symmetry coincide. Here  $c_{pq}$  are obtained from  $C_{ijkl}$  following the rule  $(11) \rightarrow 1, (12) = (21) \rightarrow 6, (22) \rightarrow 2$  and for orthotropic case additionally  $c_{16} = c_{26} = 0$ . The orthotropic in-plane case is transformed into an isotropic one if the additional relations hold:  $c_{11} = c_{22} = \lambda + 2\mu$  and  $c_{12} = \lambda, c_{66} = \mu$ , with  $\lambda$  and  $\mu$  the Lamé constants.

Under the assumption of small deformations, the strain-displacement relation for in-plane wave motion is

$$(2) \quad \varepsilon_{kl}(x, \omega) = \frac{1}{2}(u_{k,l}(x, \omega) + u_{l,k}(x, \omega)),$$

where comma subscripts denote partial differentiation with respect to the spatial coordinates and the summation convention over repeated indices is implied.

## 2.2 DYNAMIC EQUILIBRIUM EQUATION AND BOUNDARY VALUE PROBLEM

For a time-harmonic response, the equations of motion attain the form

$$(3) \quad \sigma_{ij,j}(x, \omega) + \rho \tilde{\omega}^2 u_i(x, \omega) = 0,$$

where  $\tilde{\omega}^2 = \frac{1+a(i\omega)^\alpha}{1+b(i\omega)^\alpha} \omega^2$  is square of the damped frequency and  $\rho$  is the material density.

In the case of an orthotropic material under plane strain conditions, substitution of the Zener viscoelastic model in wave equation (3), yields the following form in terms of the displacement components:

$$(4) \quad \begin{aligned} c_{11}u_{1,11}(x, \omega) + c_{66}u_{1,22}(x, \omega) + (c_{12} + c_{66})u_{2,12}(x, \omega) + \rho \tilde{\omega}^2 u_1(x, \omega) &= 0, \\ (c_{12} + c_{66})u_{1,12}(x, \omega) + c_{66}u_{2,11}(x, \omega) + c_{22}u_{2,22}(x, \omega) + \rho \tilde{\omega}^2 u_2(x, \omega) &= 0. \end{aligned}$$

The total wave field in either the  $R^2 \setminus \Gamma$  or the  $R^2 \setminus G$  domain is a superposition of the incident wave field and the wave field scattered by the crack  $\Gamma$  or  $S$ , i.e.,  $u_i(x, \omega) = u_i^{in}(x, \omega) + u_i^{sc}(x, \omega)$  and  $t_i(x, \omega) = t_i^{in}(x, \omega) + t_i^{sc}(x, \omega)$  on  $\Gamma$ . In order

to complete the BVP at the macro-scale, we add the boundary condition directly along crack line  $\Gamma$

$$(5) \quad t_i(x, \omega) = 0, \quad \text{i.e.} \quad t_i^{sc}(x, \omega) = -t_i^{in}(x, \omega), \quad x \in \Gamma.$$

At the nano-scale along the surface  $S$  of the blunt nano-crack, we have the non-classical boundary condition proposed by [1] that takes into consideration a jump in the stresses as one moves from the bulk material (matrix  $M$ ) to the crack surface due to the presence of surface stress  $\sigma_{ij}^S$  along  $S$ , see Fig. 1b. We now have that  $\sigma_{ij}^S = \tau_0 \delta_{ij} + \frac{\partial E}{\partial \varepsilon_{ij}^S}$ , where  $E$  is the deformation-dependent surface energy density,  $\varepsilon_{ij}^S$  is the strain tensor at surface  $S$ ,  $\delta_{ij}$  is the Kronecker delta symbol, and finally  $\tau_0$  is the residual surface tension under unstrained conditions along the undeformed surface, which induces an additional static deformation. The residual surface tension  $\tau_0$  is usually ignored in dynamic analysis, because its static nature does not influence on the dynamic response of the solid under consideration. It is assumed that the surface layer  $S$  has zero thickness, but is otherwise elastic and isotropic with surface Lamé constants  $\lambda^S$  and  $\mu^S$  whose numerical values are nowadays available in the literature. Additionally, it is assumed that the interface  $S$  is a coherent, perfectly bonded layer, where the strain  $\varepsilon_{ll}^S$  in the tangential direction is equal to the tangential strain in the bulk matrix, i.e.,  $\varepsilon_{ll}^S = \varepsilon_{ll}^M$ . In this case, the condition  $\varepsilon_{ll}^S = \frac{u_n}{\rho} + \frac{\partial u_l}{\partial l}$  is satisfied, see [1], where  $\rho$  is the curvature radius of the boundary  $S$ .

More specifically, the following conditions for the stresses are satisfied along the tangential and normal directions of  $S$ , i.e., the local coordinate system of normal  $n$  and tangential  $l$  vector components along the interface  $S$ , see [53, 55]:

$$(6) \quad \begin{cases} \sigma_{nl}^M = -\frac{\partial \sigma_{ll}^S}{\partial l}, & \text{on } S, \\ \sigma_{nn}^M = \frac{\sigma_{ll}^S}{\rho}, & \text{on } S, \end{cases}$$

where  $\sigma_{ll}^S = (\lambda^S + 2\mu^S)\varepsilon_{ll}^S$ .

The boundary condition (6) can be written with respect to the tractions developed along  $S$ , see [50, 52] as follows:

$$(7) \quad \begin{pmatrix} t_1^M \\ t_2^M \end{pmatrix} = T^S \begin{pmatrix} u_1 \\ u_2 \end{pmatrix} \quad \text{on } S,$$

where  $T^S = T_1 + \frac{\partial}{\partial l}T_2 + \frac{\partial^2}{\partial l^2}T_3$  and

$$\begin{aligned}
 T_1 &= \frac{1}{\varrho^2} N \begin{pmatrix} -\alpha^S & 0 \\ -\alpha^S \varrho_{,l} & 0 \end{pmatrix} N', & N &= \begin{pmatrix} n_1 & -n_2 \\ n_2 & n_1 \end{pmatrix}, \\
 T_2 &= N \begin{pmatrix} 0 & -\beta^S \\ \beta^S & 0 \end{pmatrix} N', & T_3 &= N \begin{pmatrix} 0 & 0 \\ 0 & \alpha \end{pmatrix} N'.
 \end{aligned}$$

In the above  $\alpha^S = \lambda^S + 2\mu^S$ ,  $\beta^S = \frac{1}{\varrho} \alpha^S$ ,  $n_i = -n_i^M$ , and  $\frac{\partial}{\partial l}$ ,  $\frac{\partial^2}{\partial l^2}$  are the first and second tangential derivatives, with traction  $t_k^M = \sigma_{kj}^M n_j$ . Note that when  $\lambda^S = \mu^S = 0$ , the boundary condition (7) degenerates to the classical boundary condition (5) describing the traction free surface of a macro-crack.

In sum, the BVP comprises the wave equation (4), with either the boundary condition (5) for a finite line macro-crack, see Fig. 1a, or the boundary condition (7) for a finite blunt nano-crack, see Fig. 1b, plus Sommerfeld's radiation condition for the scattered wave field at infinity.

### 3 BIEM FORMULATION

There are three main components to a BIEM formulation in elastodynamics: the incident wave load on the crack boundary; the displacement and traction fundamental solution pair of the governing equation in the viscoelastic plane; and the integro-differential equation along the crack boundary.

#### 3.1 INCIDENT WAVE

In order to solve the BVP formulated in Section 2, the incident wave displacement field at an observer point  $x$ , at a fixed frequency  $\omega$  and direction of propagation  $\eta = (\eta_1, \eta_2)$ ,  $\eta_1 = \cos \varphi$ ,  $\eta_2 = \sin \varphi$  in the elastic anisotropic plane must be known. Proceeding as in [26], we obtain for the incident displacement wave field the following expression:

$$(8) \quad u_i^{in}(x, \omega) = p_i^j(\eta) e^{-ik_j(x, \omega) \langle x, \eta \rangle},$$

where  $\langle \cdot, \cdot \rangle$  denotes the scalar product in  $R^2$ . Next, the complex wave numbers are denoted as  $k_j(x, \omega) = \tilde{\omega} \sqrt{\frac{\rho}{\vartheta_j(\eta)}}$ ,  $Re(\tilde{\omega}) > 0$ ;  $\vartheta_j(\eta) > 0$ ,  $\vartheta_1(\eta)\vartheta_2(\eta)$  and  $p_j(\eta) = (p_j^1(\eta), p_j^2(\eta))$  respectively are the eigenvalues and eigenvectors of the matrix

$$\begin{pmatrix} c_{11}\eta_1^2 + c_{66}\eta_2^2 + 2c_{16}\eta_1\eta_2 & c_{16}\eta_1^2 + c_{26}\eta_2^2 + (c_{12} + c_{66})\eta_1\eta_2 \\ c_{16}\eta_1^2 + c_{26}\eta_2^2 + (c_{12} + c_{66})\eta_1\eta_2 & c_{66}\eta_1^2 + c_{22}\eta_2^2 + 2c_{26}\eta_1\eta_2 \end{pmatrix}.$$

In (8), index  $j = 1$  stands for a P- and  $j = 2$  is for SV-incident waves.

Note that for the isotropic case  $\vartheta_1 = \lambda + 2\mu$ ,  $\vartheta_2 = \mu$  and that  $\vartheta_j$  and  $p_j$  do not depend on the wave propagation direction  $\eta$ . The tractions produced by the incident wave along the crack line  $\Gamma$  or crack boundary  $S$  are obtained as  $t_i^{in}(x, \omega) = \sigma_{ij}^{in}(x, \omega)n_i$ , with  $n = (n_1, n_2)$  the outward normal vector to  $\Gamma^+$  or  $S$  and the constitutive law between  $\sigma_{ij}^{in}(x, \omega)$  and  $\varepsilon_{ij}^{in}(x, \omega)$  was given in (1).

### 3.2 FUNDAMENTAL SOLUTION

The fundamental solution of the partial differential equation (3) is a matrix-valued function  $u_{ij}^*(x, \xi, \omega)$  satisfying the system of equations

$$C_{ijkl}u_{km,lj}^* + \rho\tilde{\omega}^2 u_{im}^* = -\delta_{im}\delta(x, \xi).$$

This fundamental solution has been derived following [26], by using the Radon transform for the case of general anisotropic continua. The difference here is that the real parameter  $\omega$  is now replaced with its complex form  $\tilde{\omega}$ , in which case we have to use the properties of cosine and sine functions with complex arguments.

### 3.3 INTEGRO-DIFFERENTIAL EQUATIONS

The formulation (3), (5) for the macro-crack and its extended version (3), (7) for the blunt nano-crack, plus Sommerfeld's radiation condition for both BVP cases, are now reformulated as an equivalent integro-differential equation along the crack line  $\Gamma$  and the interface  $S$ , respectively. Traction BIE are derived following [25, 26] based on the two-state conservation integral of elastodynamics.

#### 3.3.1 THE MACRO-CRACK

At the macroscopic level, we have the following formulation:

$$(9) \quad t_i^{in}(x, \omega) = C_{ijkl}n_j(x) \int_{\Gamma^+} \left[ \left( \sigma_{p\eta k}^*(x, \xi, \omega) \Delta u_{p,\eta}^{sc}(\xi, \omega) - \rho\omega^2 u_{pk}^*(x, \xi, \omega) \Delta u_p^{sc} \right) \delta_{\lambda l} - \sigma_{m\lambda k}^*(x, \xi, \omega) \Delta u_{m,l}^{sc}(\xi, \omega) \right] n_\lambda(\xi) d\xi, \quad x \in \Gamma,$$

where  $u_{ij}^*$  is a displacement fundamental solution and  $\sigma_{ijk}^* = C_{ijml}u_{mk,l}^*$  is the corresponding stress.

The above traction BIE (10) is a frequency-dependent, non-hypersingular equation with respect to the unknown crack opening displacement (COD) of the scattered wave field defined as  $\Delta u_i^{sc} = u_i^{sc}|_{\Gamma^+} - u_i^{sc}|_{\Gamma^-}$ ,  $i = 1, 2$ . For numerical solution of this integro-differential equation is applied a numerical scheme developed in [25] and based on the discretization and collocation procedure discussed in Section 4. All singular integrals after discretization of the BIE (10) converge in the Cauchy principal-value (CPV) sense, if a priori smoothness requirements are fulfilled, see [26].

Once solution for the COD along the crack  $\Gamma$  is recovered, the solution for displacements and stresses at any point  $x \in R^2 \setminus \Gamma$  can be obtained by the respective use of the following integral representation formulae

$$u_j^{sc}(x, \omega) = - \int_{\Gamma^+} \sigma_{kij}^*(x, \xi, \omega) \Delta u_k^{sc}(\xi, \omega) n_i(\xi), \quad x \notin \Gamma,$$

$$\sigma_{pq}^{sc}(x, \omega) = -C_{pqkl} \int_{\Gamma^+} \sigma_{ijk,l}^*(x, \xi, \omega) \Delta u_i^{sc}(\xi, \omega) n_j(\xi), \quad x \notin \Gamma,$$

Finally, the total wave field is obtained by the superposition formulae discussed in Section 2.2.

Next, the computation of SIFs is based on the well-known traction formulae, see [63]. Consider, for example, a crack along the segment with local coordinates for the end points as  $(-c, 0)$  and  $(c, 0)$  in the plane  $x_3 = 0$ , see Fig. 1a. The SIFs are computed from fractions at the crack-tips as

$$K_I = \lim_{x_1 \rightarrow \pm c} t_2(x_1, 0) \sqrt{2\pi(x_1 \mp c)}; \quad K_{II} = \lim_{x_1 \rightarrow \pm c} t_1(x_1, 0) \sqrt{2\pi(x_1 \mp c)}.$$

The normalized dynamic SIFs are given as  $K_I^* = |K_I/\sigma\sqrt{\pi c}|$ ,  $K_{II}^* = |K_{II}/\sigma\sqrt{\pi c}|$ , where  $\sigma = \omega\sqrt{\rho c_{22}}$ .

### 3.3.2 THE BLUNT NANO-CRACK

The integro-differential equation with respect to the scattered wave displacements along the interface  $S$ , together with the non-classical boundary conditions and Sommerfeld's radiation condition at infinity, which comprises the BVP in the case of blunt nano-crack, is as follows:

$$(10) \quad c_{ij}(t_j^{in}(x, \omega) - t_j^M(x, \omega)) = C_{ijkl} n_j(x) \int_S \left[ (\sigma_{p\eta k}^*(x, \xi, \omega) u_{p,\eta}^{sc}(\xi, \omega) - \rho\omega^2 u_{pk}^*(x, \xi, \omega) u_p^{sc}(\xi, \omega)) \delta_{\lambda l} - \sigma_{m\lambda k}^*(x, \xi, \omega) u_{m,l}^{sc}(\xi, \omega) \right] n_\lambda(\xi) d\xi, \quad x \in S.$$

where  $u_i^M = u_i^{sc} + u_i^{in}$ ,  $t_i^{in} + t_i^{sc} = t_i^M$ , and  $c_{ij}$  is a jump term depending on the local geometry at the source point  $x$ .

Following standard discretization and collocation procedures with respect to Eq. (16) and satisfaction of the non-classical boundary conditions (7), the resulting solution now takes into consideration the effects of surface elasticity via the Gurtin–Murdoch model. As in the case of the macro-crack, once the numerical solution to BIE (16) is recovered for a fixed frequency  $\omega$ , the displacements and tractions produced by the scattered wave field added to the incident field, yields the total wave

field in the viscoelastic anisotropic plane. Then, the normalized SCF  $F_I^* = |F_I|$ ,  $F_{II}^* = |F_{II}|$  on  $S$  at the point  $(c, 0)$  is evaluating using the formulae

$$(11) \quad \begin{aligned} F_I((x_1, 0), \omega) &= \frac{\sigma_{22}((x_1, 0), \omega)}{\sigma_{22}^{in}((x_1, 0), \omega)} \sqrt{2\pi(x_1 - c)}, \quad x_1 > c, \\ F_{II}((x_1, 0), \omega) &= \frac{\sigma_{12}((x_1, 0), \omega)}{\sigma_{22}^{in}((x_1, 0), \omega)} \sqrt{2\pi(x_1 - c)}, \quad x_1 > c. \end{aligned}$$

In [64, 65] and [66] is shown that asymptotic fields in the blunt-crack problems exhibit square root singularity even in the case of extremely narrow blunt cracks. Many authors conclude that the asymptotic behavior near the nano-crack-tip is still unknown and needs to be further investigated [59, 67]. In the paper by [68] is shown that the Gurtin-Murdoch theory as applied to fracture reduces the crack-tip singularity from the square-root singularity to a logarithmic singularity. A large number of studies have been conducted over time based on the linear fracture mechanics concept, both experimentally and theoretically for a wide range of specimen sizes, from meters to micrometers. The problem for fracture of nano-materials is still under development and there is no clear answer about the stress singularity at the nano-crack tips. In [57] is investigated the influences of surface energy on the stress distributions near a blunt crack tip for Mode I and Mode III cracks by using a local analysis method and they calculate stress concentration factor by using the formulae given by Eq. (18). In our work we would like to illustrate the sensitivity of the stress concentration field to mutual play of surface elasticity effect, anisotropy and viscoelasticity assuming that the principles of linear fracture mechanics still hold.

#### 4 NUMERICAL IMPLEMENTATION AND PARAMETRIC STUDIES

The numerical scheme for solution of both BVPs presented above by the integro-differential equations (10) over line  $\Gamma$  for a macro-crack (Fig. 1a) and (16) over interface  $S$  for a blunt nano-crack (Fig. 1b) is implemented by application of standard collocation and discretization procedures. The non-hypersingular traction BIEs are collocated on one side of the line crack boundary using displacement jumps COD as unknowns in the case of a macro-crack. In the case of the blunt nano-crack, the nodal collocation is along both sides of the interface surface. The displacements and tractions are approximated with parabolic shape functions which satisfy Hölder continuity, at least at the collocation points, while the COD shows an asymptotic-type  $O(\sqrt{r})$  behaviour near the crack tips. Quarter-point boundary elements (BE) are implemented in the case of the macro-crack. The disadvantage of the standard quadratic BE approximation regarding the smoothness at all irregular points is overcome by the shifted point method, see [26]. Following discretization, the resulting integrals are

at least CPV integrals. More specifically, at first the regular integrals are computed employing standard Gaussian quadrature for one-dimensional integrals and a Monte Carlo integration scheme for two-dimensional integrals. Next, all integrals with singular kernels are solved analytically in a small neighbourhood around the field point, using the approximation of the fundamental solutions for a small arguments. After discretization of the non-hypersingular traction BIEs, an algebraic system of equations with respect to the unknowns is obtained and solved by matrix inversion. To this end, software codes based on the Mathematica 6.0 software package have been programmed to implement the above described procedure.

To classify the types of problems under consideration, the macro-crack  $\Gamma$  is a segment  $(-c, c)$  along the  $Ox_1$  axis and  $c = 5 \times 10^{-3}$  m, where the first and fifth elements modeling this crack are quarter-point crack-tip BE with a length of  $0.15c$ . For the blunt nano-crack  $S$  with  $c = 5 \times 10^{-9}$  m and corresponding length  $|S| = 2.04281 \times 10^{-8}$  m, we use 10 ordinary BE distributed as eight along  $S^- \cup S^+$  and two on the semi-circle  $S^l, S^r$  with radius  $d = 0.0375c$ .

The resulting SIF are normalized by the static value modes  $K_I^*$  and  $K_{II}^*$  and are evaluated for the normalized frequency  $\Omega = c\omega\sqrt{\rho/c_{22}}$ . The material density of the bulk medium containing either the macro-crack or the nano-crack is  $\rho = 2.4 \times 10^3$  kg. In addition, we consider an orthotropic material with material parameter values, see [69], given as a ratio of  $\gamma$ , i.e.,  $c_{ij} = \alpha_{ij}\gamma$  with  $\gamma = 6.6495$  GPa. More specifically, the material constants used in the numerical examples, with  $\alpha_{16} = \alpha_{26} = 0$  in all cases, are as follows:

- a) an isotropic material (labeled type 1) with  $\alpha_{11} = 1, \alpha_{12} = 1/3, \alpha_{22} = 1, \alpha_{66} = 1/3$ ;
- b) an orthotropic material (labeled type 2) with  $\alpha_{11} = 1, \alpha_{12} = 1/3, \alpha_{22} = 1, \alpha_{66} = 1/6$ ;
- c) an orthotropic material (labeled type 3) with  $\alpha_{11} = 1, \alpha_{12} = 1/30, \alpha_{22} = 1, \alpha_{66} = 1/3$ .

The first set of numerical results generated by the BIEM formulation for these two simple configurations of a single crack at the macro-level and then at the nano-level are now given. At first, Fig. 2 shows the frequency behaviour of the normalized SIF  $K_I^*$  near the line macro-crack  $\Gamma$  under a normally-incident time-harmonic P-wave propagating in an orthotropic viscoelastic plane. The material is described by the Zener constitutive law with the model constant  $\alpha = 0.5$  which is a value in between a zero order derivative and a first order one. The following values of the coefficients  $a$  and  $b$  are used:  $a = b = 1$ , as this case corresponds to the pure elastic material

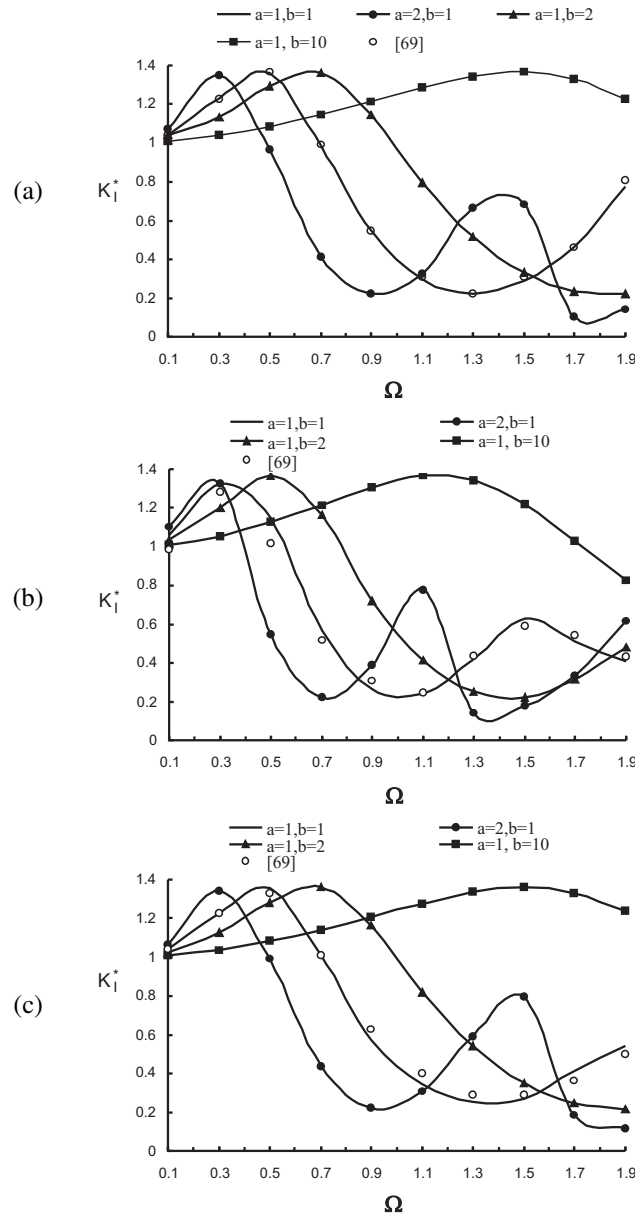


Fig. 2. Normalized SIF  $K_I^*$  versus non-dimensional frequency  $\Omega$  for a macro-crack under normal incident P-wave propagating in viscoelastic plane of Zener type with  $\alpha = 0.5$  and different values for constants  $a$  and  $b$ : (a) isotropic material of type 1; (b) orthotropic material of type 2; (c) orthotropic material of type 3.

without viscosity;  $a = 1, b = 2$ ;  $a = 2, b = 1$  and  $a = 1, b = 10$ . Fig. 2a is for comparing the linear elastic with the viscoelastic isotropic material of type 1, while Figs. 2b and 2c are for the elastic and viscoelastic orthotropic materials of type 2 and type 3, respectively. In Fig. 2, the results for the purely elastic material ( $a = b = 1$ ) are gauged for accuracy by comparison with analytical solutions obtained by [69]. Thus, case  $a = b = 1$  in Fig. 2 establishes the accuracy of our BIEM numerical scheme as applied to solution of in-plane wave problems involving cracks. Next, we focus on viscoelastic anisotropic materials (Zener model) with a macro-crack. To the author's best knowledge, there are no results available in the open literature for a crack in an anisotropic viscoelastic material described by the Zener model. It is well known that the presence of anisotropy distorts the stress field that develops in the bulk material as compared to the isotropic reference case, and this depends on the incoming wave's incidence angle. Also, as the frequency increases, the normalized stress intensity factor first oscillates upwards and then starts to drop rather rapidly in value as compared to the static case of  $K_I^* = 1$ . What is interesting to observe is the superimposed effect of material viscosity. We see that there are combinations of the two viscoelastic parameters ( $a, b$ ) for which the shift of the stress intensity curve is to the right (1, 2) and to the left (2, 1) of the reference undamped curve, and this varies with the amount of anisotropy. What is more unusual is that in one viscoelastic case (1, 10) the stress intensity factor is nearly constant with frequency, especially for the isotropic bulk material. This type of behavior obviously has consequences in the design or in the performance of components that are expected to crack under service loads.

Next we explore the question of incident elastic wave angle on the stress intensity factors. Fig. 3, 4 plot the normalized SIFs  $K_I^*$  and  $K_{II}^*$  versus normalized frequency  $\Omega$  for a macro-crack under time-harmonic incident P- and SV- wave correspondingly, propagating in viscoelastic isotropic plane of the Zener type with  $\alpha = 0.5$  and different values of coefficients  $a$  and  $b$  in the fractional Zener model. More specifically, all of Figs. 2 – 4 clearly show the sensitivity of the dynamic SIFs to the wave type (P- or SV- wave), to the wave propagation direction, to the presence of anisotropy, and more important, to the presence of viscoelasticity. Focusing on Figs. 3 and 4, we observe the importance of the wave incidence angle on the  $K_I^*$  and  $K_{II}^*$  factors (the latter being smaller in numerical value than the former and exhibiting less oscillations with increasing frequency) for the isotropic material. In the absence of viscous behavior, these results are well known. However, as viscosity is allowed to develop, the pattern previously observed emerges: There are ( $a, b$ ) viscoelastic parameter combinations for which the stress intensity factor frequency curve shifts to the right (1, 2) and to the left (2, 1) of the reference elastic curve. However when this parameter combination is (1, 10), the stress intensity curves are nearly constant with frequency. This type of

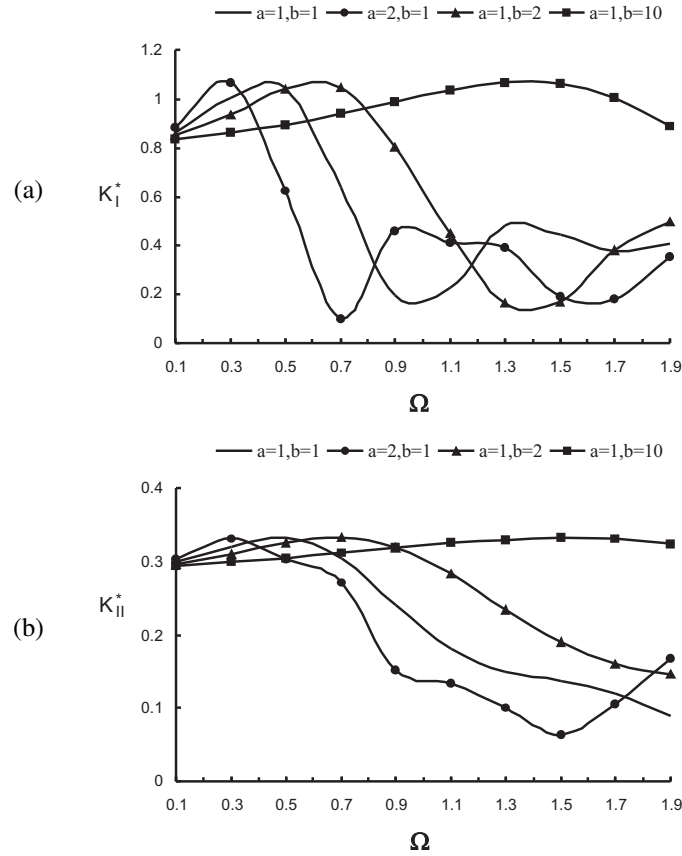


Fig. 3. Normalized SIFs versus non-dimensional frequency  $\Omega$  at the right crack-tip of a line macro-crack subjected to incident P-wave with incident angle  $\varphi = \pi/3$  in a viscoelastic isotropic plane of Zener type with  $\alpha = 0.5$  and different values for  $a$  and  $b$ : (a)  $K_I^*$ ; (b)  $K_{II}^*$ .

response is consistent in all cases plotted above, be it P- or SV- incident waves. To summarize, increasing the coefficient  $a$  value with respect to coefficient  $b$ , the maximum values of the SIFs move to lower frequencies, while the opposite effect, namely increasing coefficient  $b$  values with respect to coefficient  $a$ , shifts the maximum values of the SIFs to the higher frequency range. This is to be expected, since a simple explanation is that coefficient  $a$  is related to the stress tensor, i.e., produces a stiffness effect, while coefficient  $b$  is related to the strain tensor, i.e., adds flexibility. Finally, a large  $b$  coefficient value is reminiscent of the Maxwell fluid.

Next, we move to the nano-scale, where it is known that surface effects become quite pronounced along the crack edges. In the numerical results now produced

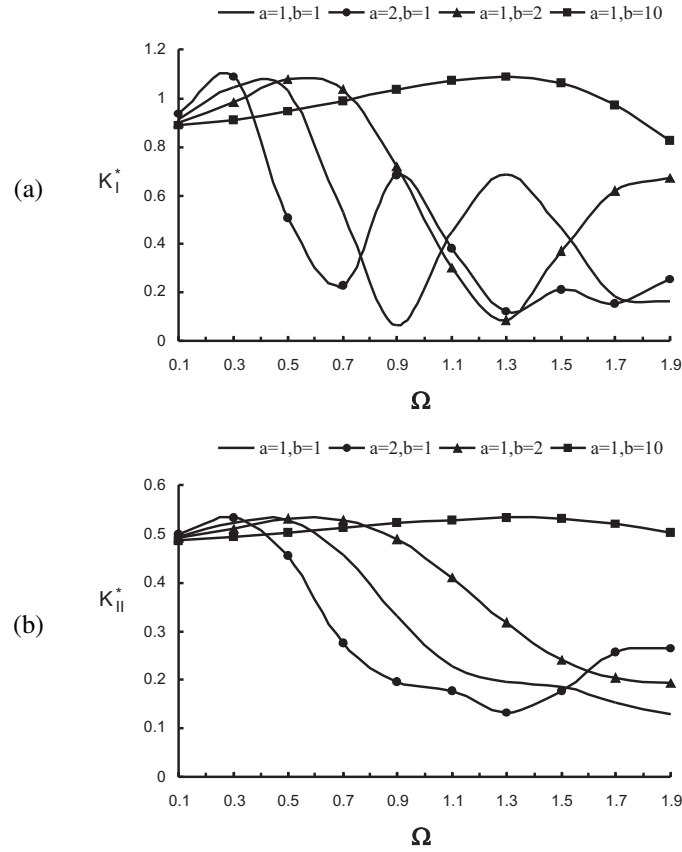


Fig. 4. Normalized SIFs versus non-dimensional frequency  $\Omega$  at the right crack-tip of a line macro-crack subjected to incident SV-wave with incident angle  $\varphi = \pi/3$  in a viscoelastic isotropic plane of Zener type with  $\alpha = 0.5$  and different values for  $a$  and  $b$ : (a)  $K_I^*$ ; (b)  $K_{II}^*$ .

for the blunt nano-crack, a dimensionless surface parameter defined as  $s = \frac{\alpha^S}{2\mu d d_s}$  is introduced, where  $\alpha^S = 6.091$  N/m,  $\mu = \gamma/3 = 2.2165 \times 10^{10}$  N/m<sup>2</sup> with  $d_s = 0.73, 18, \infty$ . Note that the case  $s = 0$  corresponds to the blunt crack without surface effects and the results degenerate to those for the macro-crack. The values of  $\alpha^S$  are taken from the literature and are usually determined by either atomic simulation techniques or experiments. In our case, these values fall within the interval  $(-10, 10)$  N/m, see [70].

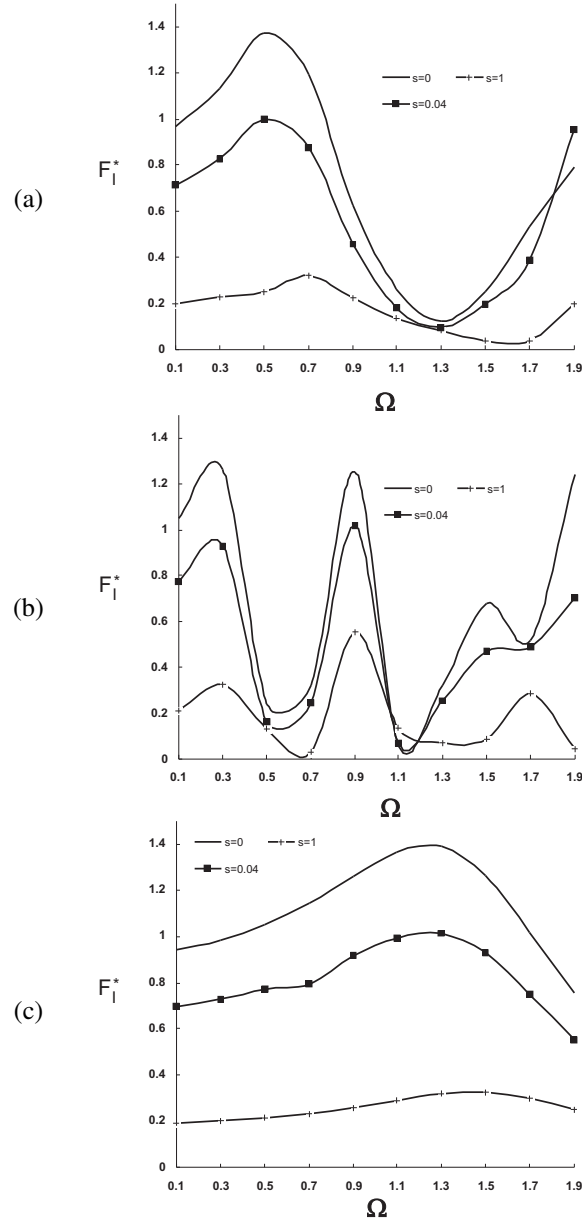


Fig. 5. Normalized SCF  $F_I^*$  for blunt nano-crack for different values of the surface elasticity parameter  $s$  versus non-dimensional frequency  $\Omega$  for a normally incident P-wave in isotropic material of type 1 with the following constants of the Zener viscoelastic model:  $\alpha = 0.5$  and (a)  $a = b = 1$ , i.e., pure elastic material; (b)  $a = 5, b = 1$ ; (c)  $a = 1, b = 5$ .

Continuing with Fig. 5, we plot the normalized SCF defined by (18) for a blunt nano-crack for three values of the surface elasticity parameter  $s = 0; s = 0.04, s = 1$ , versus normalized frequency  $\Omega$ . The input is a time-harmonic incident P-wave propagating in the following bulk material configurations:

- a) elastic isotropic continua, see Fig. 5a;
- b) viscoelastic isotropic continua described by Zener model with model constants given as  $a = 5; b = 1, \alpha = 0.5$ , see Fig. 5b;
- c) viscoelastic isotropic continua described by Zener model with model constants given as  $a = 1; b = 5, \alpha = 0.5$ , see Fig. 5c.

As previously mentioned, the case  $s = 0$  corresponds to the macro-crack, because the surface elasticity effect is neglected. Thus, the results in Fig. 5a for  $s = 0$  are the same as those in Fig. 2 for the isotropic elastic material, i.e., Zener model with constants  $a = b = 1$ . This serves as a check on the BIEM implementation at the nano-scale. As parameter  $s$  increases, the values of the stress intensity factor for the incident P-wave starts to drop across the entire frequency range. In fact, at  $s = 1$ ,  $F_I^*$  attains only 20% of its value had surface effects been absent. This behavior is consistent as the bulk material becomes viscoelastic. More specifically, the  $(a, b)$  combination of  $(5, 1)$  indicates a stiffer (Kelvin solid) type of model, while the combination  $(1, 5)$  points towards a Maxwell fluid. Thus,  $F_I^*$  is more oscillatory with frequency in the former case, as compared to the elastic case, while in the latter case,  $F_I^*$  is nearly flat indicating small dependence on the incoming wave frequency.

In Fig. 6 we now show results pertaining to the normalized SCF for a blunt nano-crack with the same values as before for the surface elasticity parameter ( $s = 0; s = 0.04, s = 1$ ) versus normalized frequency  $\Omega$  for a plane time-harmonic P-wave propagating in an orthotropic bulk material of type 3. More specifically, Fig. 6a is for pure elastic case, while Fig. 6b is for viscoelastic orthotropic continua described by the Zener model with sets of constants  $(a = 5, b = 1)$  and derivative order  $\alpha = 0.5$ . Also Fig. 6c is again for the viscoelastic Zener model with constants  $(a = 1, b = 5)$  and derivative order  $\alpha = 0.5$ . As before, results in Fig. 6a for  $s = 0$  fully degenerate to the results in Fig. 2c for  $a = b = 1$  at the macro-level. The close agreement between results in Fig. 5a and Fig. 6a for  $s = 0$  with those obtained by [69] demonstrates the high accuracy and convergence of BIEM solutions in the prescribed frequency intervals. Next, by comparing Fig. 5 and 6, it is possible to ascertain the influence of bulk material anisotropy on the stress concentration factor  $F_I^*$  for an incident P-wave. It is seen that there are somewhat more fluctuations occur in the  $F_I^*$  frequency response as compared to the isotropic material case, but these seem to be relatively minor.

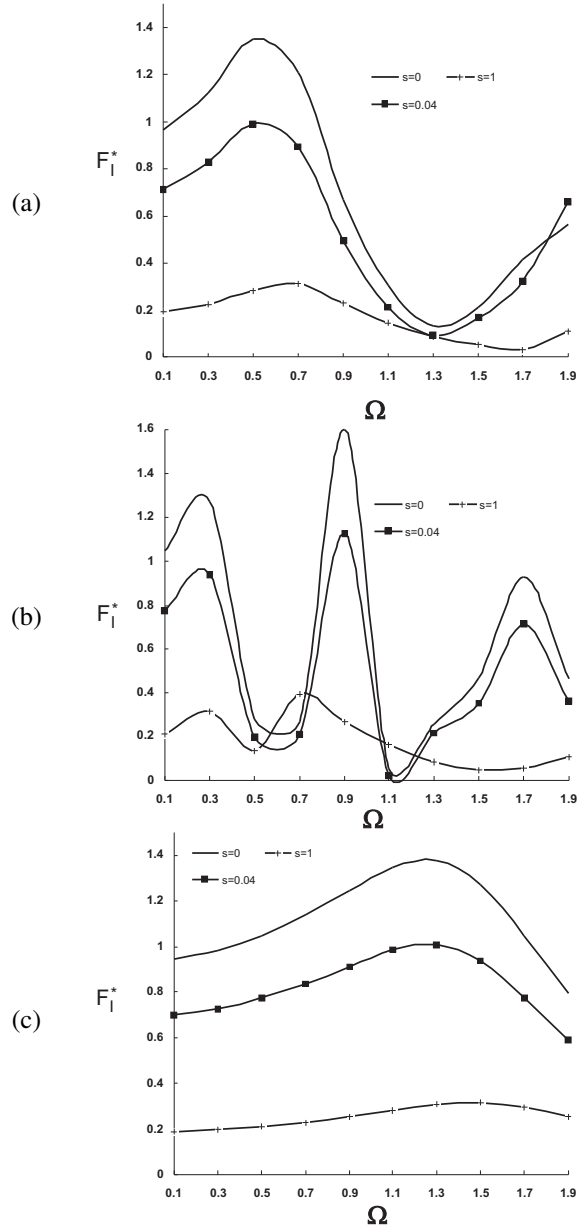


Fig. 6. Normalized SCF  $F_I^*$  for blunt nano-crack for different values of the surface elasticity parameter  $s$  versus non-dimensional frequency  $\Omega$  for a normally incident P-wave in orthotropic material of type 3 with the following constants of the Zener viscoelastic model:  $\alpha = 0.5$  and (a)  $a = b = 1$ , i.e., pure elastic material; (b)  $a = 5, b = 1$ ; (c)  $a = 1, b = 5$ .

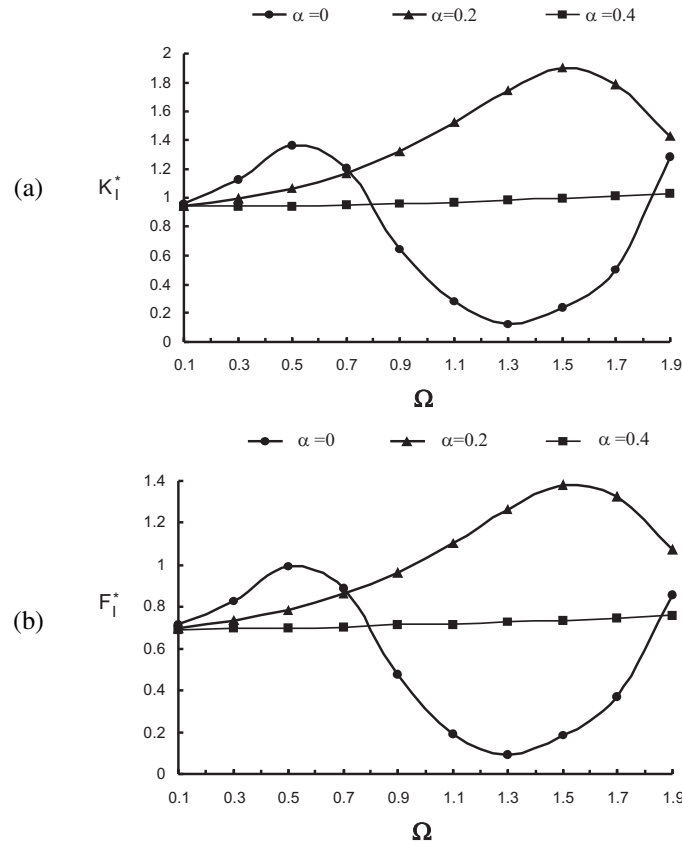


Fig. 7. Normalized SIF  $K_I^*$  and SCF  $F_I^*$  versus non-dimensional frequency  $\Omega$  for a normal incident P-wave with the following constants of the Zener viscoelastic model:  $a = 0.0002$ ,  $b = 0.02$  for isotropic material of type 1 and values of  $\alpha = 0, 0.2, 0.4$  for: (a) macro-crack; (b) blunt nano-crack with  $s = 0.04$ .

Thus, compared to the influence of surface and viscous effects on  $F_I^*$ , the influence of anisotropy is rather minor.

Finally, we move to examine the difference between the normalized SIF  $K_I^*$  for a macro-crack and the SCF  $F_I^*$  for a blunt nano-crack as a function of the surface parameters versus normalized frequency  $\Omega$  in Figs. 7a, b, respectively. This comparison is for a normally incident P-wave propagating in an isotropic viscoelastic plane with fixed Zener model parameters  $a = 0.0002$  and  $b = 0.02$ . Three different curves are shown for three different values of the derivative order  $\alpha$  in the Zener model. It can be seen that the stress concentration quantities are extremely sensitive to parameter  $\alpha$  and its influence become stronger at higher frequencies. At first, the stress inten-

sity response of the crack is consistent as one moves from the macro- to the nano-scale. For  $\alpha = 0$ , we have the most oscillatory response. As this parameter increases, the viscoelasticity effect becomes more prominent and the response starts to dampen out. In fact, when the viscoelastic material is described by  $\alpha = 0.4$ , the  $K_J^*$  is almost insensitive to the frequency variation. However, at the nano-scale, surface effects further reduce the stress intensity at the crack tip, with values in the range of 80% of what is observed at the macro-scale.

In closing, this brief parametric study clearly demonstrates the sensitivity of the dynamic stress concentration fields in a bulk material containing a single, stationary crack to the following key factors in terms of ascending importance: (i) type and characteristics of the dynamic load; (ii) material anisotropy; (iii) the manifestation of viscoelasticity and (iv) size effect and surface elasticity phenomena.

## 5 CONCLUSIONS

This work focuses on the time-harmonic analysis of a viscoelastic, orthotropic plane containing a crack at either the macro- or at the nano-scale. The analysis is carried out using a non-hypersingular, traction BIE formulation with a frequency-dependent fundamental solution of the underlying wave equation for the time-fractional Zener viscoelastic medium, as obtained by the Radon transform. As the fundamental solution of the governing wave equation is derived for a case of general anisotropy, the proposed numerical scheme can be extended beyond orthotropic materials used in the numerical examples to other types of anisotropic materials. For a nano-crack is introduced the surface elasticity model of [1], with the interface regarded as an elastic, isotropic and infinitesimally thin membrane. The membrane itself adheres to the surface of an opening without slippage and with elastic properties different from those of the surrounding bulk material. The BIE formulation is implemented numerically by discretizing the crack boundary using standard nodal collocation. Furthermore, the formulation is verified through comparisons with results obtained by other methods. Next, numerical simulations show that the stress concentration field developing near a crack in a bulk material under plane strain conditions is strongly influenced by the presence of viscoelasticity, the specific type of material anisotropy, the propagating elastic wave characteristics, the size of the crack, plus the wave-crack interaction. These results find application in the fields of computational fracture mechanics, non-destructive testing evaluation, as well as in the reliability analysis of structural elements and components. Also, the strong influence of the size effect when looking at nano-cracks can significantly alter the overall effective dynamic fracture behaviour of nano-composites. Thus, we observe that viscoelastic anisotropic materials containing nano-cracks behave quite differently from what is observed at the macro-scale. More specifically, the strain energy can be dramatically altered by surface effects,

and hence the local and macroscopic properties of the material change, a fact that must be taken into account in nano-technology applications.

#### ACKNOWLEDGEMENT

The authors acknowledge the support of the Bilateral Bulgarian Greek Project between BAS and AUTH.

#### REFERENCES

- [1] GURTIN, M. E., A. I. MURDOCH. A Continuum Theory of Elastic Material Surfaces. *Arch. Ration. Mech. Anal.*, **57** (1975), 291-323.
- [2] SCHANZ, M. Wave Propagation in Viscoelastic and Poroelastic Continua: A Boundary Element Approach, Lecture Notes in Applied Mechanics, Vol. 2, Springer, Berlin, 2001.
- [3] BOLTZMANN, L. Theorie der elastischen nachwirkungen. *Sitzungsbericht der Akademie der Wissenschaften (Wien): Mathematisch-Naturwissenschaftlichen Klasse*, **70** (1874), No. 2, 275-300.
- [4] MEYER, O. E. Theorie der inneren Reibung. *J. Reine Ang. Math.*, **78** (1974), 130-135.
- [5] CHRISTENSEN, R. M. Theory of Viscoelasticity, Academic Press, New York, 1971.
- [6] FLUGGE, W. Viscoelasticity, Springer-Verlag, New York, 1975.
- [7] KOBAYASHI, S., T. KAWAKAMI. Application of BE-FE Combined Method to Analysis of Dynamic Interaction between Structures and Viscoelastic Soil. In C. A. Brebbia and G. Maier, editors, *Boundary Elements VII*, vol. I, Berlin, Springer-Verlag, 1985, pp. 6-3-6-12.
- [8] MANOLIS, G. D., D. E. BESKOS. Dynamic Stress Concentration Studies by Boundary Integrals and Laplace Transform. *Int. J. Numer. Meth. Eng.*, **17** (1981), 573-599.
- [9] CAPUTO, M. Vibrations of an Infinite Plate with a Frequency Independent. *Q. J. Acoust. Soc. Am.*, **60** (1976) No. 3, 634-639.
- [10] BAGLEY, R. L., P. J. TORVIK. A Theoretical Basis for the Application of Fractional Calculus to Viscoelasticity. *Journal of Rheology*, **27** (1983), No. 3 201-210.
- [11] GAUL, L., P. KLEIN, M. PLENGE. Dynamic Boundary Element Analysis of Foundation Slabs on Layered Soil. In C. A. Brebbia, editor, *Boundary Elements X*, vol. 4, Southampton, Computational Mechanics Publication, 1988, pp. 29-44.
- [12] ROSSIKHIN, Y. A., M. V. SHITIKOVA. Applications of Fractional Calculus to Dynamic Problems of Linear and Nonlinear Hereditary Mechanics of Solids. *Appl. Mech. Rev.*, **50** (1997), No. 1, 15-67.
- [13] PODLUBNI, I. Fractional Differential Equations, Academic Press, New York, 1999.
- [14] CAPUTO, M., F. MAINARDI. Linear Models of Dissipation in Anelastic Solids. *II Nuovo Cimento, Ser. II*, **1** (1971) 161-198.
- [15] MESHKOV, S. Description of Internal Friction in the Memory Theory of Elasticity Using Kernels with a Weak Singularity. *Zh. Prikl. Mekh. Tekh. Fiz.*, **8** (1967), 147-151.

- [16] HOLM, S., S. P. NÄSHOLM. A Causal and Fractional All-Frequency Wave Equation for Lossy Media. *J. Acoust. Soc. Am.*, **130** (2011), 2195-2202.
- [17] ATANACKOVIC, T. M., M. JANEV, L. OPARNICA, S. PILIPOVIC, D. ZORICA. Space-time Fractional Zener Wave Equation. *Proc. R. Soc. A*, **471** (2015), 20140614.
- [18] CAPUTO, M. Linear Model of Dissipation Whose Q Is Almost Frequency Independent – II. *Geophys. J. R. Astron. Soc.*, **13** (1967), 529-539.
- [19] ROSSIKHIN, Y. A., M. V. SHITKOVA. Application of Fractional Calculus for Dynamic Problems of Solid Mechanics: Novel Trends and Recent Results. *Appl. Mech. Rev.*, **63** (2010), 1-52.
- [20] ATANACKOVIC, T. M., S. KONJIK, L. OPARNICA, D. ZORICA. Thermodynamical Restrictions and Wave Propagation for a Class of Fractional Order Viscoelastic Rods. *Abstr. Appl. Anal.*, **32** (2011), ID 975694.
- [21] CAI, W., W. CHEN, W. XU. Characterizing the Creep of Viscoelastic Materials by Fractal Derivative Models. *Int. J. Non-Linear Mech.*, **87** (2016), 58-63.
- [22] XU, H., X. JIANG. Creep Constitutive Models for Viscoelastic Materials Based on Fractional Derivatives. *Comput. Math. Appl.*, **73** (2017), No 6, 1377-1384.
- [23] ZHAN, R. T., Z. X. LI, L. WANG. A Fractional Differential Constitutive Model for Dynamic Stress Intensity Factors of an Anti-Plane Crack in Viscoelastic Materials. *Acta Mech. Sinica*, **30** (2014), No. 3, 403-409.
- [24] ZHURAVKOV, M. A., N. S. ROMANOVA. Review of Methods and Approaches for Mechanical Problem Solutions Based on Fractional Calculus. *Math. Mech. Solids*, **21** (2016) No. 5, 595-620.
- [25] ZHANG, C., D. GROSS. On Wave Propagation in Elastic Solids with Cracks, Comput. Mech. Publ., Southampton, 1998.
- [26] DINEVA, P., D. GROSS, R. MÜLLER, T. RANGELOV. Dynamic Fracture of Piezoelectric Materials. Solutions of Time-harmonic Problems via BIEM, Solid Mechanics and its Applications, v. 212, Springer Int. Publ., Switzerland, 2014.
- [27] MANOLIS, G. D., P. S. DINEVA. Elastic Waves in Continuous and Discontinuous Geological Media by Boundary Integral Equation Methods: A Review. *Soil Dyn. Earthq. Eng.*, **70** (2015), 11-29.
- [28] GURTIN, M. E., A. I. MURDOCH. Surface Stress in Solids. *Int. J. Solids Str.*, **14** (1978), 431-440.
- [29] GURTIN, M. E., J. WEISSMÜLLER, F. LARCHE. A General Theory of Curved Deformable Interfaces in Solids at Equilibrium. *Philos. Mag. A*, **78** (1998), 1093-1109.
- [30] LUO, J., X. WANG. On the Anti-Plane Shear of an Elliptic Nano Inhomogeneity. *Europ. J. Mech. /A Solids*, **28** (2009), 926-934.
- [31] WANG, G. F., T. J. WANG. Deformation Around a Nanosized Elliptical Hole with Surface Effect. *Appl. Phys. Letters*, **89** (2006) 161901.
- [32] MOGILEVSKAYA, S. G., S. L. CROUCH, H. K. STOLARSKI. Multiple Interacting Circular Nano-Inhomogeneities with Surface/Interface Effects. *J. Mech. Phys. Solids*, **56** (2008) 2298-2327.

- [33] MOROZOV, N. F., B. N. SEMENOV. Selected Problems of Nanomechanics. *Sci. Publ. State Univ. Novi Pazar, Ser. A: Appl. Math. Inform. Mech.*, **5** (2013), 1-6.
- [34] WANG, S., M. DAI, C. Q. RU, C. F. GAO. Stress Field Around an Arbitrarily Shaped Nanosized Hole with Surface Tension. *Acta Mech.*, **225** (2014), 3453-3463.
- [35] YANG, Q., J. X. LIU, X. Q. FANG. Dynamic Stress in a Semi-Infinite Solid with a Cylindrical Nano-Inhomogeneity Considering Nanoscale Microstructure. *Acta Mech.*, **223** (2012) 879-888.
- [36] QIANG, F. W., P. J. WEI, X. Q. LIU. Propagation of Elastic Wave in Nanoporous Material with Distributed Cylindrical Nanoholes. *Sci. China-Phys. Mech. Astron.*, **56** (2013), 1542-1552.
- [37] WANG, G. F. Multiple Diffraction of Plane Compressional Waves by two Circular Cylindrical Holes with Surface Effects. *J. Appl. Phys.*, **105** (2009), 013507-013509.
- [38] WANG, G. F., T. J. WANG, X. Q. FENG. Surface Effects on the Diffraction Of Plane Compressional Waves by a Nanosized Circular Hole. *Appl. Phys. Lett.*, **89** (2006), 231923-1-231923-3.
- [39] FANG, X. Q., J. X. LIU, J. X. YANG, L. L. ZHANG. Effect of Surface/Interface on the Dynamic Stress of Two Interacting Cylindrical Nano-Inhomogeneities under Compressional Waves. *Thin Solid Films*, **518** (2010), 6938-6944.
- [40] RU, Y., G. F. WANG, T. J. WANG. Diffraction of Elastic Waves and Stress Concentration Near a Cylindrical Nano-Inclusion Incorporating Surface Effect. *J. Vib. Acoust.*, **131** (2009), No. 6, 061011-1-061011-7.
- [41] TIAN, L., R. K. N. D. RAJAPAKSE. Elastic Field of an Isotropic Matrix with a Nanoscale Elliptical Inhomogeneity. *Int. J. Solids Str.*, **44** (2007), 7988-8005.
- [42] SHARMA, P., L. T. WHEELER. Size-Dependent Elastic State of Ellipsoidal Nano-Inclusions Incorporating Surface/Interface. *J. Appl. Mech.*, **74** (2017), 447-454.
- [43] FANG, X. Q., L. L. ZHANG, J. X. LIU. Dynamic Stress Concentration Around two Interacting Coated Nanowires with Surface/Interface Effect. *Meccanica*, **48** (2013), No. 2, 287-296.
- [44] OU, Z. S., D. W. LEE. Effects of Interface Energy on Scattering of Plane Elastic Wave by a Nano-Sized Coated Fiber. *J. Sound Vibr.*, **331** (2012), 5623-5643.
- [45] SODAGAR, S., A. GURAN. Interaction of Elastic Waves with a Cylindrical Nano-Inclusion. *AIP Conf. Proc.*, **1487** (2012), 248-255.
- [46] KIM, C. I., P. SCHIAVONE, C. Q. RU. The Effect of Surface Elasticity on a Mode-Iii Interface Crack. *Arch. Mech.*, **63** (2011), No. 3, 267-286.
- [47] NAN, H., B. WANG. Effect of Residual Surface Stress on the Fracture of Nanoscale Materials. *Mech. Res. Commun.*, **44** (2012), 30-34.
- [48] WU, C. H. The Effect of Surface Stress on the Configurational Equilibrium of Voids and Cracks. *J. Mech. Phys. Solids*, **47** (1999), 2469-2492.
- [49] JAMMES, M., S. G. MOGILEVSKAYA, S. L. CROUCH. Multiple Circular Nano-Inhomogeneities and/or Nano-Pores in One of Two Joined Isotropic Half-Planes. *Eng. Anal. Bound. Elem.*, **33** (2009), 233-248.

- [50] DONG, C. Y., E. PAN. Boundary Element Analysis of Inhomogeneities of Arbitrary Shapes with Surface and Interface Effects. *Eng. Anal. Bound. Elem.*, **35** (2011), 996-1002.
- [51] DONG, C. Y. An Integral Equation Formulation of Two- and Three-Dimensional Nanoscale Inhomogeneities. *Comput. Mech.*, **49** (2012), 309-318.
- [52] PARVANOV, S., G. MANOLIS, P. DINEVA. Wave Scattering by Nano-heterogeneities Embedded in a Elastic Matrix via BEM. *Eng. Anal. Bound. Elem.*, **56** (2015), 57-69.
- [53] PARVANOV, S., G. VASILEV, P. DINEVA, G. MANOLIS. Dynamic Analysis of Nano-Heterogeneities in a Finite-Sized Solid by Boundary and Finite Element Methods. *Int. J. Solids. Str.*, **80** (2016), 1-18.
- [54] PARVANOV, S., G. VASILEV, P. DINEVA. Elastodynamic Analysis of Anisotropic Elastic Solid with Multiple Nano-Cavities. *Europ. J. Comput. Mech.*, **25** (2016), No. 1-2, 129-146.
- [55] DINEVA, P., T. RANGELOV. Wave Scattering by Cracks at Macro- and Nano-Scale in Anisotropic Plane by BIEM. *J. Theor. Appl. Mech.*, **46** (2016), No. 4, 19-35.
- [56] WANG, G. F., Y. LI. Influence of Surface Tension on Mode-I Crack Tip Field. *Eng. Fract. Mech.*, **109** (2013), 290-301.
- [57] WANG, G. F., X. Q. FENG, T. J. WANG, W. GAO. Surface Effects on the Near-Tip Stresses for Mode-I and Mode-III Cracks. *ASME, J. Appl. Mech.*, **75** (2008), 011001.
- [58] FU, X. L., G. F. WANG, X. Q. FENG. Surface Effects on the Near-Tip Stress Fields of a Mode-II Crack. *Int. J. Fract.*, **151** (2008), 95-106.
- [59] FU, X. L., G. F. WANG, X. Q. FENG. Effects of Surface Elasticity on Mixed-Mode Fracture. *Int. J. Appl. Mech.*, **3** (2011), No. 3, 435-446.
- [60] HOAGLAND, R. G., M. S. DAW, J. P. HIRTH. Some Aspects of Forces And Fields in Atomic Models of Crack Tips. *J. Mater. Res.*, **6** (1991), 2565-2571.
- [61] MAINARDI, F. Fractional Calculus and Waves in Linear Viscoelasticity: An Introduction to Mathematicam Models, Imperial College Press, London, UK, 2010.
- [62] MAKROU, A. A., G. D. MANOLIS. A Fractional Derivative Zener Model for the Numerical Simulation of Base Isolated Structures. *Bull. Earthquake Eng.*, **14** (2016), No. 1, 283-295.
- [63] ALIABADI, A. M., D. ROOKE. Numerical Fracture Mechanics, Comput. Mech. Publ., Southampton, 1991.
- [64] CREAGER, M. The Elastic Stress Field Near the Tip of a Blunt Crack, Master's thesis, Lehigh University, Bethlehem, USA, 1966.
- [65] CREAGER, M., P. C. PARIS. Elastic Field Equations for Blunt Cracks with Reference to Stress Corrosion Cracking. *Int. J. Fract. Mech.*, **3** (1967), No. 4, 247-252.
- [66] OVCHARENKO, J. N. The Elastic Stress-Deformed Conditions and Density of Energy of Deformation at Top Extremely Narrow U-Notches. *Proc. Tula Uni., Technical Sci.*, **10** (2013), 1-13 (in Russian).
- [67] FU, X. L., G. F. WANG, X. Q. FENG. Surface Effects on Mode-I Crack-Tip Fields: A Numerical Study. *Eng. Fract. Mech.*, **77** (2010), 1048-1057.

- [68] SENDOVA, T., J. R. WALTON. A New Approach to the Modeling and Analysis of Fracture through Extension of Continuum Mechanics to the Nanoscale. *Math. Mech. Solids*, **15** (2010), No. **3**, 368-413.
- [69] OHYOSHI, T. Effect of Orthotropy on Singular Stresses for a Finite Crack. *ASME, J. Appl. Mech.*, **40** (1973), 491-497.
- [70] SHENOY, V. B. Size-Dependent Rigidities of Nanosized Torsional Elements. *Int. J. Solids Struct.*, **39** (2002), 4039-4052.